Bioactive Materials 10 (2022) 247–254

Contents lists available at ScienceDirect

Bioactive Materials

journal homepage: www.sciencedirect.com/journal/bioactive-materials

Modeling human hypertrophic scars with 3D preformed cellular aggregates bioprinting

Yao Bin [a,b,c,d,1], Zhu Dongzhen [a,b,1], Cui Xiaoli [e], Enhe jirigala [f,g], Song Wei [a,b], Li Zhao [a,b], Hu Tian [a,b,h], Zhu Ping [d], Li Jianjun [a,b], Wang Yuzhen [a,b], Zhang Yijie [a,b], Fu Xiaobing [a,b,**], Huang Sha [a,b,*]

[a] Research Center for Tissue Repair and Regeneration Affiliated to the Medical Innovation Research Department, PLA General Hospital and PLA Medical College, 28 Fu Xing Road, Beijing, 100853, PR China
[b] PLA Key Laboratory of Tissue Repair and Regenerative Medicine and Beijing Key Research Laboratory of Skin Injury, Repair and Regeneration, Research Unit of Trauma Care, Tissue Repair and Regeneration, Chinese Academy of Medical Sciences, 2019RU051, 51 Fu Cheng Road, Beijing, 100048, PR China
[c] Academy of Medical Engineering and Translational Medicine, Tianjin University, 300072, PR China
[d] Guangdong Cardiovascular Institute, Guangdong Provincial People's Hospital, Guangdong Academy of Medical Sciences, Guangzhou, Guangdong, 510100, PR China
[e] General Surgery Department, Yangzhou Hongquan Hospital, Jiangsu, 225200, PR China
[f] Institute of Basic Medical Research, Inner Mongolia Medical University, Hohhot, Inner Mongolia, 010110, PR China
[g] College of Graduate, Tianjin Medical University, 22 Qi Xiang Tai Road Tianjin, 300050, PR China
[h] MRC Human Immunology Unit, MRC Weatherall Institute of Molecular Medicine, University of Oxford, John Radcliffe Hospital, Oxford, OX3 9DU, UK

ARTICLE INFO

Keywords:
Hypertrophic scar model
Preformed cell aggregates
3D bioprinting
Microenvironmental cues
Drug screening

ABSTRACT

The therapeutic interventions of human hypertrophic scars (HHS) remain puzzle largely due to the lack of accepted models. Current HHS models are limited by their inability to mimic native scar architecture and associated pathological microenvironments. Here, we create a 3D functional HHS model by preformed cellular aggregates (PCA) bioprinting, firstly developing bioink from scar decellularized extracellular matrix (ECM) and alginate-gelatin (Alg-Gel) hydrogel with suitable physical properties to mimic the microenvironmental factors, then pre-culturing patient-derived fibroblasts in this bioink to preform the topographic cellular aggregates for sequent printing. We confirm the cell aggregates preformed in bioink displayed well defined aligned structure and formed functional scar tissue self-organization after bioprinting, hence showing the potential of creating HHS models. Notably, these HHS models exhibit characteristics of early-stage HHS in gene and protein expression, which significantly activated signaling pathway related to inflammation and cell proliferation, and recapitulate in vivo tissue dynamics of scar forming. We also use the in vitro and in vivo models to define the clinically observed effects to treatment with concurrent anti-scarring drugs, and the data show that it can be used to evaluate the potential therapeutic target for drug testing. The ideal humanized scar models we present should prove useful for studying critical mechanisms underlying HHS and to rapidly test new drug targets and develop patient-specific optimal therapeutic strategies in the future.

1. Introduction

Human hypertrophic scars (HHS) can significantly affect the patient's quality of life, both physically and psychologically [1]. Currently, many different types of models exist to study HHS formation, ranging from simple monolayer cell culture to 3D tissue-engineered

Peer review under responsibility of KeAi Communications Co., Ltd.

* Corresponding author. Research Center for Tissue Repair and Regeneration affiliated to the Medical Innovation Research Department, PLA General Hospital and PLA Medical College, 28 Fu Xing Road, Beijing, 100853, PR China.

** Corresponding author. PLA Key Laboratory of Tissue Repair and Regenerative Medicine and Beijing Key Research Laboratory of Skin Injury, Repair and Regeneration, Research Unit of Trauma Care, Tissue Repair and Regeneration, Chinese Academy of Medical Sciences, 2019RU051, 51 Fu Cheng Road, Beijing, 100048, PR China.

E-mail addresses: fuxiaobing@vip.sina.com (F. Xiaobing), stellarahuang@sina.com (H. Sha).

[1] These authors contributed equally to this work.

https://doi.org/10.1016/j.bioactmat.2021.09.004
Received 10 July 2021; Received in revised form 17 August 2021; Accepted 2 September 2021
Available online 8 September 2021

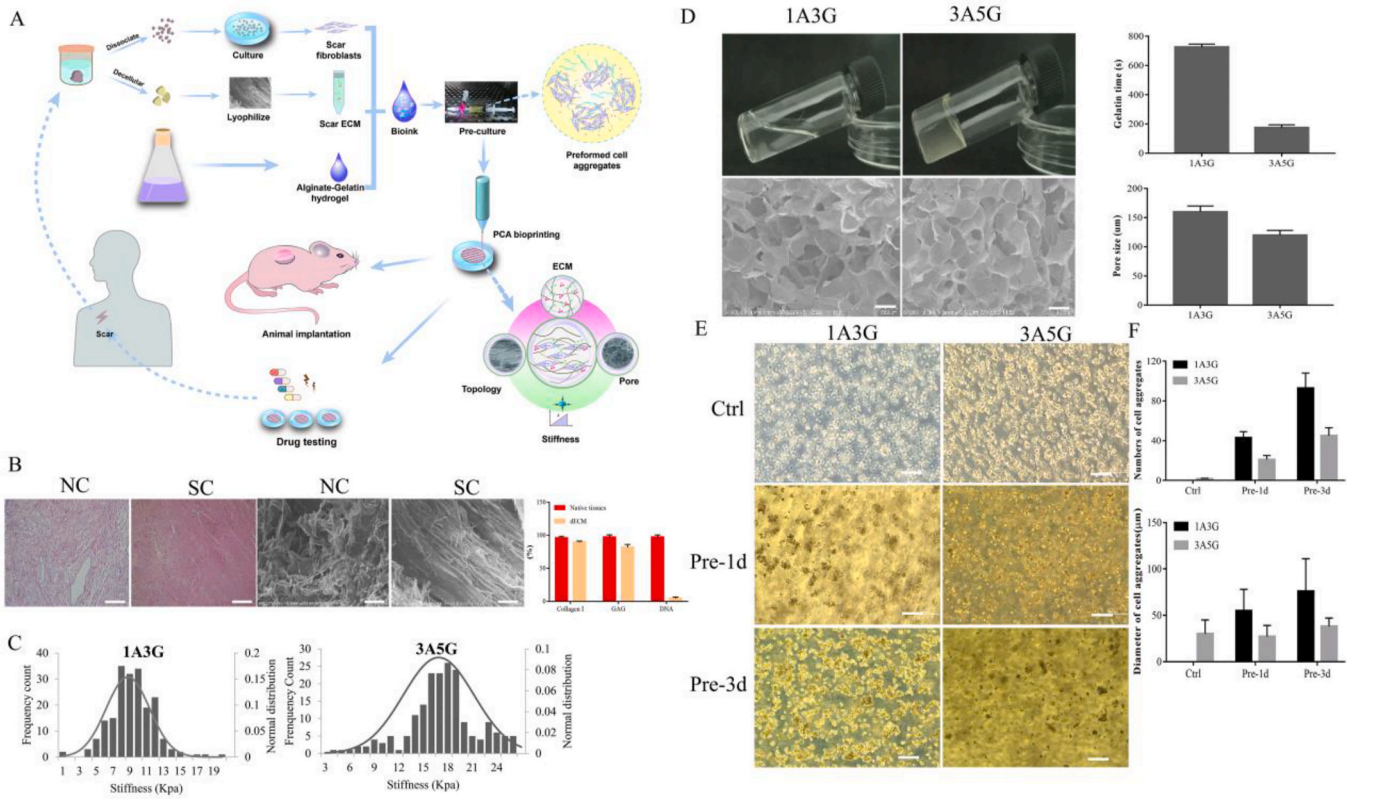

Fig. 1. Preparation of bioinks. (A) Schematic illustration of the whole process of fabrication of scar model. **(B)** HE (Scale bar = 200 μm) and SEM images (Scale bar = 100 μm) of normal dECM and scar dECM and components of native tissue and dECM. **(C)** Local mechanical strength of different bioinks. **(D)** Gelation of hydrogels and SEM images of bioinks (scale bar = 500 μm) and the related statistics. **(E)** Formation of cell aggregates in different bioinks with different culture time (scale bar = 200 μm). **(F)** Statistical analysis of diameters and numbers of cell aggregates under different pre-culture conditions (n = 3).

models even to humanized mouse models. However, HHS is unique to humans, and interspecies differences make it impossible of animal models to recapitulate the features of human biology and human disease. Even with ongoing research in this field, current models do not fully recapitulate human scarring and therapeutic approaches remain clinically unsatisfactory [2]. Additionally, the majority of cells would lose fibrotic phenotypes and topological arrangement upon 2D culture conditions. This discrepancy contributed to the high failure rate in drug treatment option [3].

Recent advancements in 3D bioprinting technologies have facilitated the construction of clinically relevant biomimetic tissues, which are able to replicate the delicate architecture and complex composition of different cells and applied for tissue regeneration [4]. Specifically, 3D in vitro constructs offer the requirement of microenvironmental factors (e.g., mechanical forces, spatial orientation, as well as oxygen, nutrient and signaling gradients) that 2D monolayers lacked [5]. We have previously developed a 3D-printed matrix to mimic the sweat gland regenerative microenvironment that directed mesenchymal stem cells (MSCs) differentiation and guided the formation and function of glandular tissue [6]. Extracellular matrix (ECM) components have been found to be useful in providing both biochemical and biophysical cues during bioprinting [7]. HHS is the accumulation of ECM components in the dermis, leading to compromised function and altered architecture [8]. Persistent activation of myofibroblasts aggravates HHS due to ECM remodeling and altered paracrine functions [9]. Therefore, we contained the scar decellularized ECM (dECM) in bioink that contribute to mimic native scar architecture and associated pathological microenvironments.

Furthermore, previous reports have demonstrated that physical factors (e.g., topology, stiffness, and pore size) represent a driving force for complex biological activities, including cell proliferation, differentiation and migration [10,11]. Scar tissue is much stiffer than normal skin, and recent evidence also suggests that matrix stiffening, which is generally regarded as an outcome of disease, may be a contributing factor in disease development [12]. Similarly, the pore size appears to be of major importance in tissue reaction and scar formation, and a previous study demonstrated that application of scaffolds with an average pore size (120 μm) resulted in more myofibroblasts activation [11]. Consequently, controlling the initial conditions to mimic the scar microenvironmental factors and developing bioink toward desired patterning outcomes are of paramount importance.

Alginate-gelatin (Alg-Gel) hydrogels have been extensively used as bioink in extrusion-based bioprinting, and all these exceptional properties make Alg-Gel based hydrogel a promising bioink for 3D bioprinting scar model [13]. In contrast to 2D cell cultures that normally acquire a flattened morphology, cells in 3D environments form more physiologically relevant multicellular structures. However, cells in hydrogels are confined, limiting their mutual interactions. Also, it is difficult to achieve the same high cell density as in native tissues [14]. To overcome these issues, we precultured cells within the bioink over a period of time before printing; in this way, cell aggregates were preformed due to high cell densities and sufficient cellular contact. We named this practical method preformed cellular aggregates (PCA) bioprinting. Different from conventient cell printing, PCA bioprinting provided a more hospitable environment for sequent self-organization and morphogenesis to occur but without the need for sophisticated systems (Fig. 1A).

Our previous work could construct a microenvironment for stem cell differentiation while it was unable to induce tissue morphogenesis rapidly. Cell spheroids bioprinting with special organization facilitates the establishment of functional organoids due to their high cell density, whereas it is difficult to carry out because the long time to form spheroid, the low capability of structural reorganization, and the

requirement of a delicate instrument for bioprinting [15,16]. To tackle these issues, PCA bioprinting was easy to perform and could promote the construction of a functional scar model facilitating drug screen. Taking advantage of PCA bioprinting, we demonstrated the topographic arrangement of cellular aggregates were able to form the aligned structure of HHS tissue. Cells in HHS model exhibited the similar expression profile with scar tissue at gene and protein level, which exhibited the potential therapeutic target for drug testing and the anti-scarring treatment assay. After transplantation, these tightly regulated cellular self-organization programs within 3D constructs would orchestrate dynamic interactions between cells and their environments, ensuring the scar development in vivo. As expected, incorporated precise small molecular drugs screened according to the results of gene set enrichment analysis (GSEA) within the bioink, would weaken the scar formation more efficiently than widely used anti-scarring drugs both in vitro and in vivo. Thus, this novel HHS model might be act as a platform to better study the scar biology and likely to offer a new avenue for drug testing and potentially increase the speed of drug development and success rates of drug candidates for anti-scarring.

2. Materials and methods

2.1. Human subjects

All human samples were collected from the Chinese PLA General Hospital (Beijing, China) with the informed consent of the patients, and the experiments were approved by the Ethics Committee of the Chinese PLA General Hospital (approval number ChiCTR2000033157).

2.2. Cell extraction and culture

First, epidermis and hypodermis of scar tissue was removed mechanically by scalpel and remanent dermis was minced to 1 mm^3 pieces in sterile culture dishes. Then, the pieces were transferred in 60 mm culture dishes which were washed by pure fetal bovine serum (FBS; 10437028, Gibco) in advance and incubated in complete DMEM (DMEM; SH30243.01, Hyclone) medium for 7days. Then, the minced tissue pieces were removed and adhered cells were continued to be incubated for 7d until the cells reached 70–80% confluence. Cells were cultured in a humidified atmosphere of at 37 °C with 5% CO_2 and harvested at 70–80% confluence. Passage 2–10 were used for following experiment.

2.3. Preparation of decellularized extracellular matrix

Epidermis and hypodermis of scar tissue was removed physically and remanent dermis was chopped into dimensions of 3mm × 3 mm.The chopped scar tissues were treated with 1 wt % Triton-X-100 and 1 wt % Sodium dodecyl sulfate (SDS) solution in phosphate buffer saline (PBS) solution at 4 °C overnight. Then scar tissues were rinsed in PBS solution for 24h to get rid of the detrimental detergent. Finally, the samples were dissolved in 0.5 M acetic acid solution containing 15 mg of pepsin per 100 mg dECM for 5days. DECM were then filtered and sterilized through a 0.22 μm filter and the pH value of dECM bioink was adjusted to 7.2 with 1 M sodium hydroxide (NaOH) solution.

2.4. Preparation of bioinks

To optimize the concentration and ratio of sodium alginate (Alg, Sigma, 75–100 kDa, guluronic acid 39%, America) and gelatin (Gel, Sigma, 96 kDa, type B, America), the printability, stiffness and pore size were measured. The Alg-Gel hydrogel was steriled by bathing at 70 °C for 30min and cooled at 4 °C for 5min for three times, then stored at 4 °C for subsequent experiments. Collagen I was added into bioinks at a concentration of 1ml/20 ml before printed. The composite hydrogels were crosslinked with 2.5% w/v calcium chloride solution for 10min at room temperature.

2.5. Establishment and evaluation of 3D-bioprinted scar model

According to the printability, stiffness and pore size of bioinks, as well as capability of cell aggregation and cell sedimentation during preculture, 3A5G hydrogel was used to establish 3D-bioprinted scar model and 1A3G hydrogel was used as control group. Three groups of bioinks, namely 1A3G hydrogel mixed with scar Fb and dECM (1SS), 3A5G hydrogel blended with scar Fb (3AS) and 3A5G hydrogel mixed with scar Fb and dECM (3ASS), were used for further study. 1ASS and 3ASS were compared to investigate the effect of stiffness and porosity on scar formation. 3AS and 3ASS were compared to investigate the effect of dECM on scar formation.

2.6. Preparation of aligned cell-laden 3D structure

We used alginate/gelatin/collagen composite hydrogel as bioinks and cells was mixed with bioinks at the concentration of 1×10^7/ml. To establish aligned cell-laden 3D structure, cell-laden bioinks were precultured in syringes for 3ds. After preculturing, the cell-laden bioinks were printed by extruded bioprinter (Regenovo 3D Bioprinter, China) with a 340 μm nozzle and moving speed of 10 mm/s and then crosslinked with 2.5% w/v calcium chloride solution for 10min at room temperature.

2.7. Proteomics analysis

Proteomics of scar dECM and normal skin dECM involved use of isobaric tags for relative and absolute quantification (iTRAQ) in Novogene Company, with differentially expressed proteins detected in scar dECM versus normal skin dECM. Two-fold greater difference in expression was considered significant.

2.8. RNA sequencing

Total RNA was prepared with Trizol (Invitrogen) and RNA-seq was performed using HiSeq 2500 (Illumina) in Novogene company. Genes with FDR<0.05, fold-difference>2.0, and mean log intensity>2.0 were considered to be significant.

2.9. Drug screening

3D-bioprinted scar model was treated with Abemaciclib (CDK4/6 inhibitor, MCE), Cobimetinib (MEK1/2 inhibitor, MCE) and Triamcinolone acetonide (glucocorticoid for clinical application, KUNMIN JIDA). To mimic drug treatment of local injection in scar lesion, 3ASS bioink were mixed with Abemaciclib (1 μM, diluted with DMSO), Cobimetinib (1 μM, diluted with DMSO),1%wt/v Triamcinolone acetonide and 0.1% v/v DMSO as control group.

2.10. Establishment and evaluation of in vivo scar model

3D-bioprinted scar model (3A5G), 3ASS with Cobimetinib (3A-C), and 3ASS with Triamcinolone acetonide (3A-T) were tranferred into nude mice after cultured for 3days. Then mice were killed after 14 days; feet were excised and fixed with 10% formalin (Sigma-Aldrich, USA) overnight for paraffin sections and immunohistological analysis. Mice were maintained in an Association for Assessment and Accreditation of Laboratory Animal Care accredited animal facility, and procedures were performed with Institutional Animal Care and Use Committee approved protocols.

2.11. Statistical analysis

All experiments were repeated at least three times to make sure

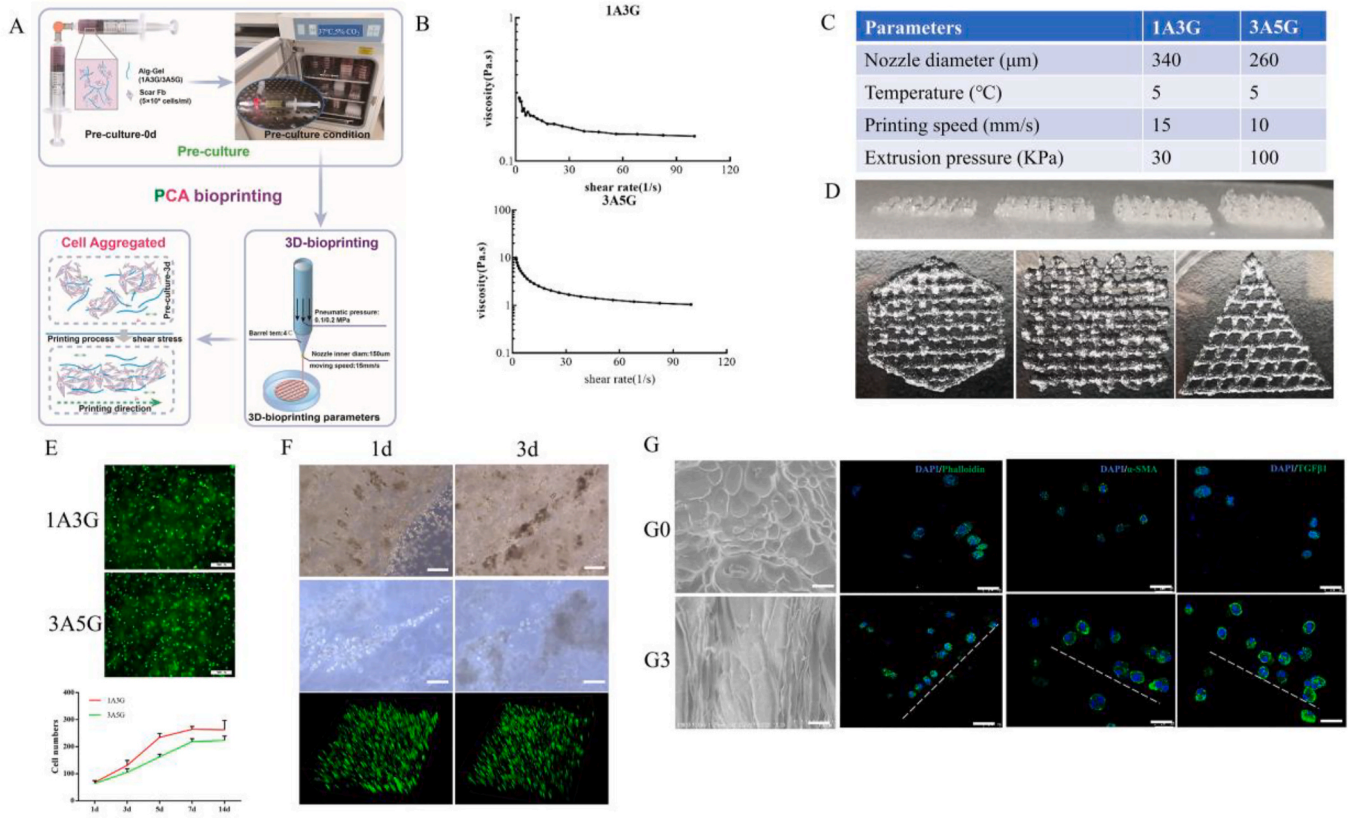

Fig. 2. Optimization of 3D printing parameters. (A) Schematic illustration of the details of PCA bioprinting. **(B)** Rheological properties of pre-cultured bioinks (n = 3). **(C)** Optimized printing parameters for pre-cultured bioink. **(D)** A lattice-shaped construct with different layers and Various 3D printed constructs. **(E)** Live/Dead staining and the proliferation rate of cells in the 3D structure (Live cells: green, Dead cells: red, scale bar = 200 μm). **(F)** Alligned cell aggregates and cell distribution in 3D printed constructs with culture. **(G)** The structure of pre-cultured 3D bioprinted constructs (Scale bar = 100 μm) and the aligned cells (Phalloidin: green, DAPI: blue, scale bar = 25 μm) and the expression of myofibroblasts markers (α-SMA, TGFβ1: green, DAPI: blue, scale bar = 25 μm). G0: without pre-culture; D3: pre-culture for 3 days. (For interpretation of the references to colour in this figure legend, the reader is referred to the Web version of this article.)

reproducibility. Differences among groups were analysed by one-way ANOVA test after testing for homoscedasticity and the data from the same group were evaluated by the Student's t-test using SPSS 23.0v software. All data were expressed as the mean ± standard and $p < 0.05$ was considered statistically significant.

3. Results and discussion

3.1. Bioink preparation and multicellular aggregates preformation

The method for prepare the bioinks with characteristics of HHS consist of a few steps. First step is decellularization of scar tissues and ECM solutions was derived from pepsin-digested decellularized tissues. HE images that cell nuclei staining was hardly detected in dECM group showed the effective removal of the double-stranded DNA content and SEM images revealed that the specific aligned structure of scar dECM and there was significant difference of the structural characteristics between native skin (NS) dECM and HHS dECM (Fig. 1B). We also estimated the proportions of collagen and glycosaminoglycans (GAGs) in ECM through hydroxyproline assay and dimethylmethylene blue assay, the collagen contents and GAGs were well retained (Fig. 1B). Then we prepared five kinds of gelatin, collagen and alginate composite hydrogels with different concentration to match the mechanical properties of NS and HHS tissues (Table S1). The overall and local mechanical strength of 1A3G and 3A5G group showed that they were similar to NS and HHS respectively (Fig. S1A; Fig. 1 C). A previous study demonstrated that application of scaffolds with an average pore size (120 μm) resulted in more myofibroblasts activation [11]. The represent SEM images showed that the pore size of bioinks of 3A5G group was just approximately 115 μm (Fig. 1D). We next investigated the rheological properties in relation to an increasing shear rate at 20 °C. The gelation time of bioink was no longer than 800s in 20 °C and with increasing shear rate, G′ and G″remained relatively stable, indicating sufficient stability of the bioink for bioprinting (Fig. 1D; Figs. S1B and C).

For cellular aggregates preformation, both 1A3G and 3A5G group could develop cell spheroids after culture, and the number and diameter of cellular aggregates of 3 day period preculture were higher than that of 1 day period preculture. Furthermore, the number and diameter of cellular aggregates in 1A3G group were higher than 3A5G group but these cellular aggregates sedimented more seriously in 1A3G group, suggesting the viscosity of 1A3G seemed inadequate for PCA bioprinting (Fig. 1E and F). Besides, uniform and smaller size of cell aggregates in 3A5G group facilitated with bioprinted process for producing low shear stress and high viability during biopriting compared to 1A3G group.

3.2. PCA bioprinting constructed aligned fibrous microstructure and increased cellular fibrotic phenotype

Tissue formation relies on a precisely regulated morphogenetic process that allows cells aggregates to locally interact and self-organize according to the guidance of tissue architecture and biochemical factors [15]. Reproducing tissue architecture and biochemical signals could ultimately provide artificial organ models to be used for drug screening or eventual tissue regeneration, lessening the burden and shorting the long times for animal testing [14]. For hypertrophic scar, the alignment of collagen network is a characteristics of scar ECM and important for

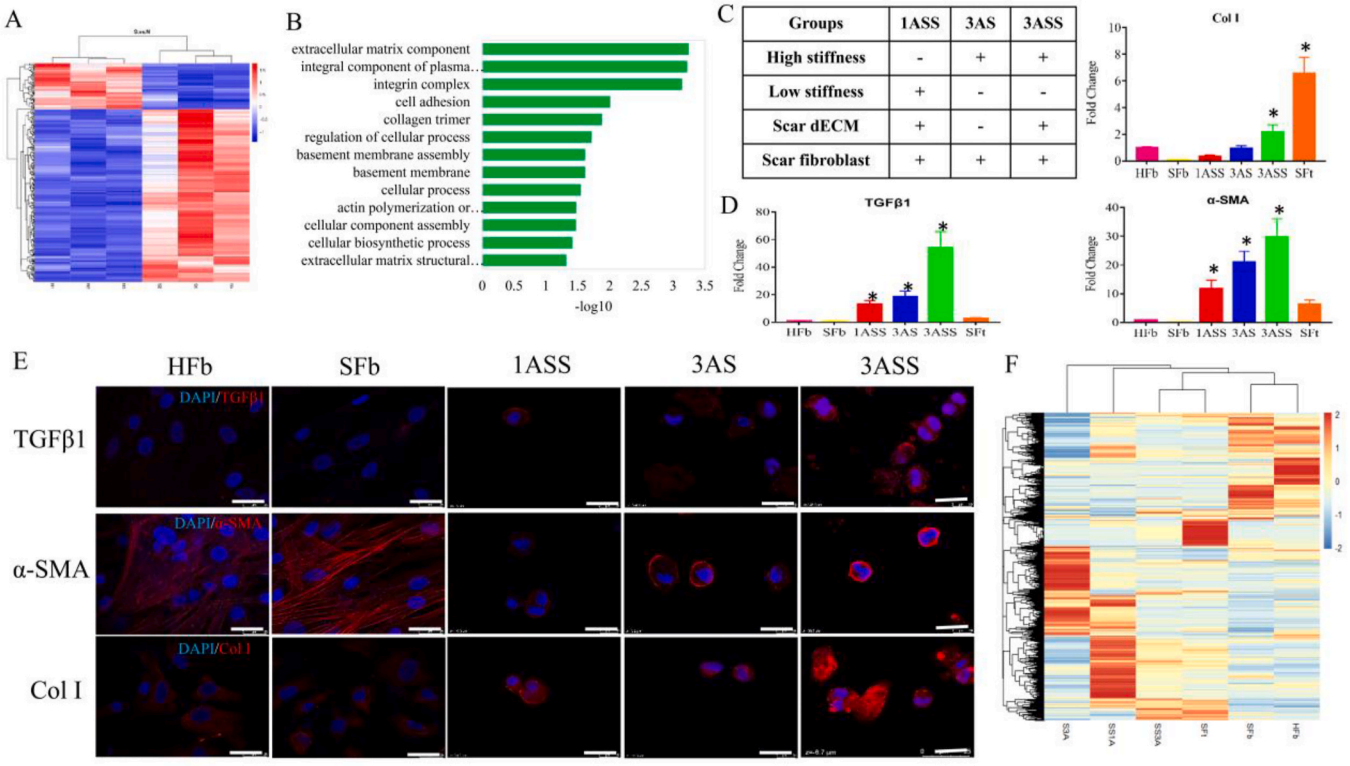

Fig. 3. Recapitulation of the pathological features of scar. (A, B) (A)The differential expression profile of normal dECM and scar dECM and **(B)** GO analysis of differentiated proteins. **(C)** The printed groups with different bioinks. **(D, E)** The expression of myofibroblast markers at gene **(D)** (Data are mean ± SEM, n = 3, $*p < 0.05$) and protein **(E)** level (α-SMA, TGFβ1, Col I: red, DAPI: blue, scale bar = 25 μm). **(F)** Transcriptional analysis of scar model with different combination of environmental cues and scar tissue. 1ASS: 1A3G+SFb+scar ECM, 3AS: 3A5G+SFb, 3ASS: 3A5G+SFb+scar ECM, SFt: scar tissue. (For interpretation of the references to colour in this figure legend, the reader is referred to the Web version of this article.)

the activity of myofibroblasts [17]. Hence, for successfully recapitulating scar tissue, the mimetic 3D micro-structure consisting of highly aligned microfibrous scaffold should be fabricated.

Bioprinting has been widely applied in tissue engineering and regenerative medicine due to its powerful ability to control large-scale depositions of cells and biocompatible materials [14,18]. Here, we established PCA bioprinting for guiding scar tissue morphogenesis across more physiologically relevant parameters and directly within highly permissive ECMs that facilitate effective multicellular self-organization (Fig. 2A).

The process of PCA bioprinting was illustrated in Fig. 2A. To obtain aligned topographical cue for enhancing the activity of myofibroblasts, cell-laden bioink was primarily pre-cultured for cell aggregates formation, then printing the structures with appropriate conditions and cell aggregates were aligned with extrusion based bioprinting direction. The structure promoted orientation alignment and activation of the embedded fibroblasts. To be specific, the 1A3G bioink originally exhibited a viscosity (η) of ≈0.2 Pa s at shear rate of ≈1s-1 and temperature of ≈15 °C, while the viscosity of 3A5G bioink was about 10 Pa s at shear rate of 1s-1 and temperature of ≈15 °C, both of them had excellent printability (Fig. 2B). Considering that pre-culture will take several days, therefore bioinks with high viscosity, which prevent cell sedimentation are advantageous for generating bioprinted constructs with homogenously distributed cells. According to the well-patterned constructs, the final printing condition was selected to be 30 kPa pressure and 15 mm.s-1 speed at 5 °C for 1A3G bioink and 100 kPa pressure and 10 mm.s-1 speed at 5 °C for 3A5G bioink (Fig. 2C). The flow of bioink extruding was smooth and the constructs after cross-linking were mechanically stable and robust, allowing to print multi-layered constructs. Lattice constructs were printed up to 10 layers (corresponding to 4 mm) and a linear relationship was obtained between the number of layers and the height of the construct. To ensure reliable printing fidelity of our bioink and printing system, constructs with complex architecture were designed and printed with different sizes and heights including a hexagon, a tetragon and a triangle lattice (Fig. 2D).

Cell viability in 3D construct was found to be sufficiently high (>90%) after cultured for 3days and the rate of cell proliferation in 3A5G group was lower than 1A3G group (Fig. 2E). Interestingly, preformed cell aggregates in PCA group could self-organize to aligned tissue architecture and cell distribution was showed. Cell aggregates developed to fibrous alignment like the structure of native scar tissue and spindle cell mass established interaction with each other to form functional fibrous tissue over cultured time (Fig. 2F). SEM images of printed construct and immunofluorescent results of cell cytoskeleton showed fibrous alignment and cells in PCA group showed upregulated expression of α-SMA and TGFβ1, the markers of myofibroblasts (Fig. 2G and H), which demonstrated the importance of tissue architecture on physiological and key factors for scar formation (Fig. 2G and H). In summary, recapitulating this factor was critical for constructing artificial organ and human pathological model.

3.3. *The biochemical and biophysical cues of scar model synergistically work on the gene and protein expression profile of fibroblasts*

Most of the previous studies demonstrated that cells in 2D culture lost normal cellular responses from morphology, proliferation, migration, and differentiation, to biochemical signaling as well as gene and protein expression [19,20]. In this study, HHS fibroblasts (SFb) of different passages didn't show obvious differences of cell morphology (Fig. S2). Although the proliferation rate and migration capability of SFb were faster than normal fibroblasts (HFb), SFb lacked the expression of myofibroblast markers in 2D culture conditions (Fig. S3). Furthermore,

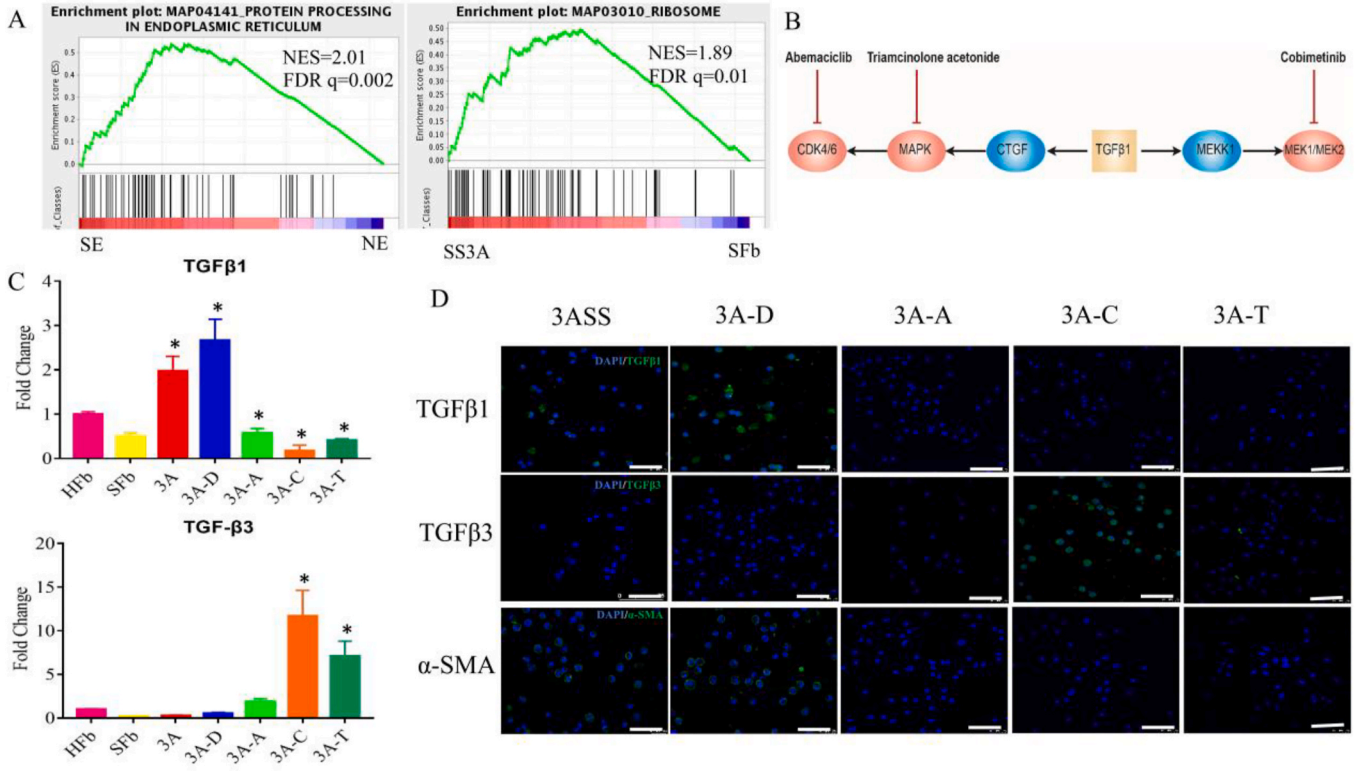

Fig. 4. Performance of predicted drugs in the bioprinted scar model. (A) The enrichment of gene sets from the GO database. **(B)** Schematic illustration of mechanism of drug screen. **(C, D)** The expression of pro-fibrotic molecule and anti-fibrotic molecule at gene **(C)** (Data are mean ± SEM, n = 3, $^*p < 0.05$) and protein **(D)** level (α-SMA, TGFβ1, TGFβ3: green, DAPI: blue, scale bar = 25 μm). 3ASS: 3A5G+SFb+scar ECM, 3A–D: 3ASS+DMSO, 3A–A: 3ASS+ Abemaciclib, 3A–C: 3ASS+ Cobimetinib, 3A–T: 3ASS+ Triamcinolone acetonide. (For interpretation of the references to colour in this figure legend, the reader is referred to the Web version of this article.)

addition of ECM form HHS in 2D condition couldn't retrieve the characteristics of myofibroblasts (Fig. S4).

We then assessed the potential of ECM addition in bioink for providing the biochemical signals of HHS microenvironments. We collected 20 HHS samples from patients with different ages (young, 5–16 years old vs. aged, 30–45 years old) (Fig. S5) and compared the effect on the recapitulation of the pathophysiology. For this comparison, we denoted the collagen in papillary dermis of HHS, the thickness, expression of type I collagen and the vascularization level of HHS were significantly different from NS but there were no differences between young and old groups ($P > 0.05$) (Fig. S6; Fig. S7; Fig. S8). We performed proteomics analysis of dECM derived from dermis of NS and HHS and the protein profile was significantly different and gene ontology (GO) enrichment analysis of differentially expressed proteins suggested that scar dECM could promote ECM organization, cellular biosynthetic process and cell division (Fig. 3A and B). However, the effect of ECM on traditional 2D condition was barely worked, which suggested the 3D spatial microenvironment was important for scar formation (Fig. S4).

We next evaluated the effect of these properties on the recapitulation of the pathophysiology of scar by comparing different combinations of environmental cues. We denoted the presence and absence of ECM as 3ASS and 3AS, and the low stiffness group was 1ASS. Each group was constructed containing SFb with PCA bioprinting (Fig. 3C). The different environmental combinations influenced the formation of the scar model. QRT-PCR and immunofluorescent staining results showed that stiffness and ECM were important for regain of myofibroblasts characteristics. Interestingly, the expression of key growth factor for scar formation-TGFβ1 and the expression of specific markers of myofibroblasts-α-SMA in the scar model were significantly higher than scar tissue, while the expression of markers of HHS-collagen I was significantly lower than scar tissue, which suggested the scar model was mostly like the initial stage of scar formation implying its potential of drug screen for preventing scar formation (Fig. 3D and E). Transcriptional analysis showed the similar results (Fig. 3F). Furtherly, GO enrichment analysis of differentially expressed proteins suggested that scar model (3ASS) combined with all factors could activated ECM secretion, ECM organization and cell division, while without stiffness (1ASS) only promoted protein translation and secretion, and without ECM (3AS) only promoted cell division, which illustrated the role of biochemical and biophysical factors in the scar model formation (Fig. S9; Fig. S10).

These results demonstrated that both of the biochemical signals like ECM proteins and biophysical factors such as tissue architecture, stiffness and pore size were critical for the myofibroblast activation, ECM secretion and remodeling and ultimate scar model formation.

These results proved that the PCA bioprinting promoted tissue self-organizaiton and significantly accelerated the construction of functional organoid or pathological model, while it is restricted by the lack of biomaterials suitable for bioink. Nonetheless, this method combined the advantages of 3D bioprinting such as precise and reproducible and the advantages of organoid such as primary cell organization and high cell density, it would proceed the development of construction of functional physiological and pathological organoids and the application of 3D bioprinting technology in tissue regeneration.

3.4. Evaluation of drug candidates in vitro and in vivo

Lastly, we demonstrated the feasibility of this model to be used for the screening of different types of drugs. Gene set enrichment analysis (GSEA) suggested that the protein processing in endoplasmic reticulum derived from the GO database is highly enriched in scar dECM compared with normal dECM, suggesting an increase in the protein secretion of HHS compared with NS. GSEA suggested that the ribosome gene set

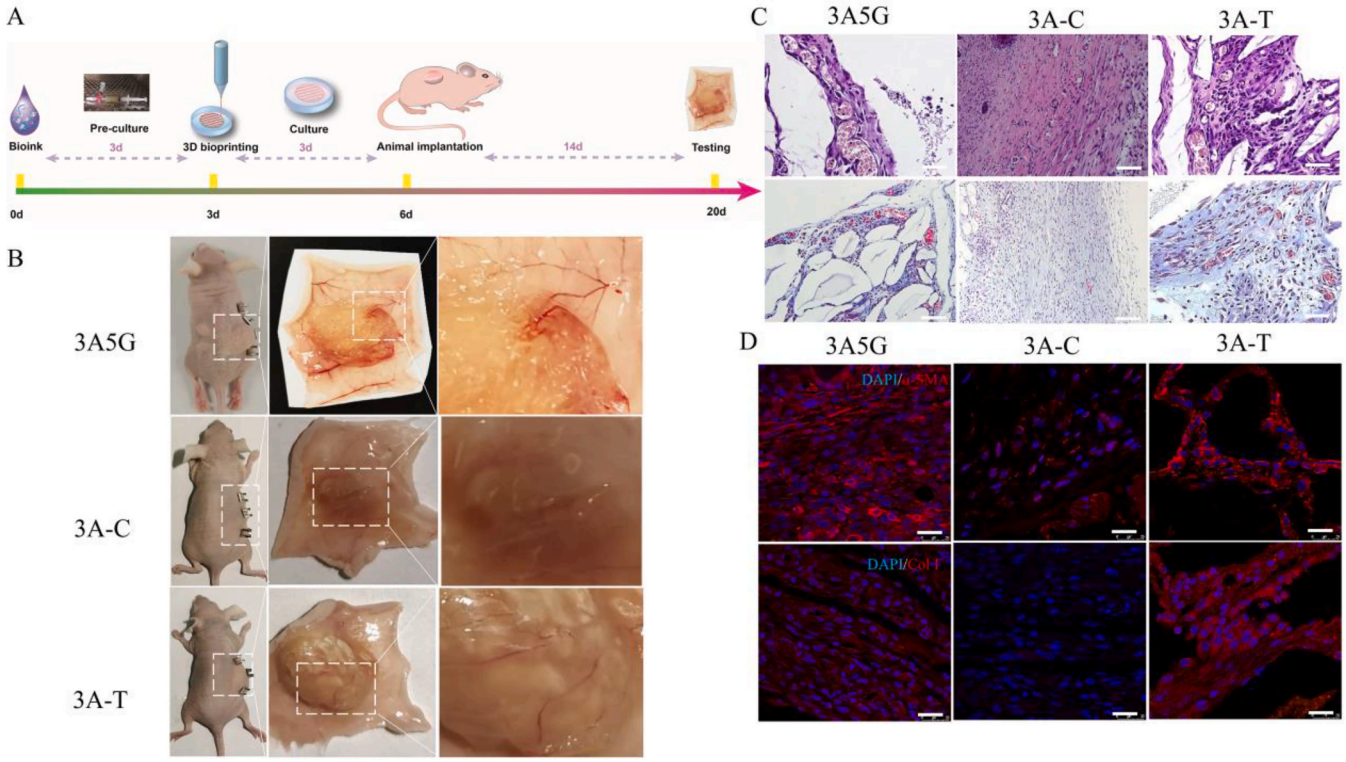

Fig. 5. Transplantation of scar model into adult immunodeficient mice displays characteristics of early stage of scar and confirmed the effect of screened drugs. (A) Schematic illustration of the whole process of animal test. **(B)** The macroscopic images of scar formation in different groups. **(C)** HE (Scale bar = 200 μm) and Masson images (Scale bar = 200 μm) of scar tissue in different groups. **(D)** The expression of myofibroblasts markers in different groups (α-SMA, Col I: red, DAPI: blue, scale bar = 100 μm). 3A5G: 3A5G+SFb+scar ECM, 3A–C: 3ASS+ Cobimetinib, 3A–T: 3ASS+ Triamcinolone acetonide. (For interpretation of the references to colour in this figure legend, the reader is referred to the Web version of this article.)

derived from the GO database is highly enriched in scar model compared with SFb, suggesting upregulation of protein synthesis of HHS compared with NS. Both of them were related to cell proliferation and GO enrichment analysis showed that cell proliferation was highly activated in scar model (Fig. 4A; Fig. S9). In light of these finding, we assumed that blocking the cell proliferation would be more effective for scar treatments. We tested two kinds of inhibitors of the cell proliferation (Abemaciclib and Cobimetinib) compared with Triamcinolone acetonide which was used for scar treatment in clinical (Fig. 4B). The results demonstrated that Cobimetinib could achieve a better effect than Triamcinolone acetonide at both gene and protein level. The profibrotic markers were significantly inhibited but the anti-fibrotic markers were activated again, which implied the success of scar model in drug screen (Fig. 4C and D).

To assess whether PCA bioprinted scar model could reproduce hypertrophic scar and the therapeutic effects of Cobimetinib in vivo, 3D printed constructs were subcutaneously implanted into adult immunodeficient mice (Fig. 5A). We transplanted a total of 6 scar models from 5 patients into 3 animals for each scar model, all of which exhibited hypertrophic scar when examined after 14days, indicating a very efficient xenograft model, whereas integrating Triamcinolone acetonide with bioprinted constructs inhibited scar formation to some extent and integrating Cobimetinib with bioprinted constructs hardly form hypertrophic scar. Macroscopic images of xenotransplanted scar tissue showed angiogenesis occurred in induced pathological tissue, resembling to the characteristics of early stage in the scar progression which was consistent with in vitro results (Fig. 5B). Histological analysis and masson staining demonstrated that 3A and 3A-T group showed angiogenesis, collagen deposition and aligned structure, while there was barely vessel formation and lower collagen fibers in 3A-C group (Fig. 5C). Immunofluorescent results of scar biomarkers showed the similar trends too (Fig. 5D). The expression of α-SMA and Col I was upregulated in 3A and 3A-T group and downregulated in 3A-C group.

Taken together, these results demonstrate that PCA bioprinted construct offers a human derived scar model recapitulating both biochemical and biophysical factors, with high similar gene expression profile with scar tissue for precisely drugs screen and high efficiency of orthotopic transplantation of engraftment for in vivo evaluation.

4. Conclusion

Our results provide proof of concept that a patient-specific hypertrophic scar model can be created through 3D bioprinting using the approach that we have described. To our best knowledge, this is the first bioprinted model that displays cell activation and ECM secretion as well as scar structure and stiffness in a single construct, which proves the suitability for bioprinted scar models to replicate the pathophysiology for drug testing. Furthermore, this bioprinted model represents the initial stage of scar formation that can be used to specifically investigate the treatment for scar prevention. In addition, the selective use of materials with different stiffness and allowed the model to generate a spatial tissue organization of scar collagen bundles. This reconstituted tissue model incorporated the main pathological features of a hypertrophic scar and the gene and protein profiles reflected biochemical and biophysical cues observed in a native hypertrophic scar. The potential application of this approach to produce a testing system personalized for individual patients is exemplified by the capability of reproducing patient-specific treatment efficacy in clinical applications.

CRediT authorship contribution statement

Yao Bin: Conceptualization, Methodology, Formal analysis, Investigation, Writing – original draft. **Zhu Dongzhen:** Conceptualization, Methodology, Formal analysis, Investigation, Visualization. **Cui Xiaoli:**

Resources. **Enhe jirigala:** Methodology, Resources. **Song Wei:** Writing – review & editing. **Li Zhao:** Methodology, Formal analysis. **Hu Tian:** Investigation, Resources. **Zhu Ping:** Investigation, Visualization. **Li Jianjun:** Resources. **Wang Yuzhen:** Writing – review & editing. **Zhang Yijie:** Methodology, Formal analysis. **Fu Xiaobing:** Supervision, Funding acquisition. **Huang Sha:** Writing – review & editing, Supervision, Project administration.

Declaration of competing interest

The authors declare no competing financial interests.

Acknowledgements

This study was supported in part by the National Nature Science Foundation of China (81830064, 81721092, 32000969, 82002056), Key Support Program for Growth Factor Research (SZYZ-TR-03), Chinese PLA General Hospital for Military Medical Innovation Research Project (CX-19026), the CAMS Innovation Fund for Medical Sciences (CIFMS, 2019-I2M-5-059), the Military Medical Research and Development Projects (AWS17J005) and National Key Research and Development Program of China (2018YFA0108700, 2017YFA0105602).

Appendix A. Supplementary data

Supplementary data to this article can be found online at https://doi.org/10.1016/j.bioactmat.2021.09.004.

References

[1] J.Q. Coentro, E. Pugliese, G. Hanley, M. Raghunath, D.I. Zeugolis, Current and upcoming therapies to modulate skin scarring and fibrosis, Adv. Drug Deliv. Rev. 146 (2019) 37.
[2] C.C. Finnerty, M.G. Jeschke, L.K. Branski, J.P. Barret, P. Dziewulski, D.N. Herndon, Hypertrophic scarring: the greatest unmet challenge after burn injury, Lancet 388 (10052) (2016) 1427.
[3] T.L. Tuan, L.S. Nichter, The molecular basis of keloid and hypertrophic scar formation, Mol. Med. Today 4 (1) (1998) 19.
[4] I. Matai, G. Kaur, A. Seyedsalehi, A. McClinton, C.T. Laurencin, Progress in 3D bioprinting technology for tissue/organ regenerative engineering, Biomaterials 226 (2020) 119536.
[5] M.A. Heinrich, W. Liu, A. Jimenez, J. Yang, A. Akpek, X. Liu, Q. Pi, X. Mu, N. Hu, R. M. Schiffelers, J. Prakash, J. Xie, Y.S. Zhang, 3D bioprinting: from benches to translational applications, Small 15 (23) (2019), e1805510.
[6] D. Kevin, M.K. Caroline, A. Adetola, Recent trends in decellularized extracellular matrix bioinks for 3D printing: an updated review, Int. J. Mol. Sci. 20 (18) (2019) 4628.
[7] B. Yao, R. Wang, Y. Wang, Y. Zhang, T. Hu, W. Song, Z. Li, S. Huang, X. Fu, Biochemical and structural cues of 3D-printed matrix synergistically direct MSC differentiation for functional sweat gland regeneration, Sci Adv 6 (10) (2020) eaaz1094.
[8] C.C. Ude, A. Miskon, R.B.H. Idrus, M.B. Abu Bakar, Application of stem cells in tissue engineering for defense medicine, Mil. Med. Res. 5 (1) (2018) 7.
[9] M.B. Piallat, G. Gabbiani, B. Hinz, The myofibroblast in wound healing and fibrosis: answered and unanswered questions, F1000Res 5 (2016) 752.
[10] M.C. Lampi, C.A. Reinhart-King, Targeting extracellular matrix stiffness to attenuate disease: from molecular mechanisms to clinical trials, Sci. Transl. Med. 10 (422) (2018), eaao0475.
[11] B.K.H.L. Boekema, M. Vlig, L.O. Damink, E. Middelkoop, L. Eummelen, A. V. Buhren, M.M.W. Ulrich, Effect of pore size and cross-linking of a novel collagen-elastin dermal substitute on wound healing, J. Mater. Sci. Mater. Med. 25 (2) (2014) 423.
[12] H. Zhu, J. Li, Y. Li, Z. Zheng, H. Guan, H. Wang, K. Tao, J. Liu, Y. Wang, W. Zhang, C. Li, J. Li, L. Jia, W. Bai, D. Hu, Glucocorticoid counteracts cellular mechanoresponses by LINC01569-dependent glucocorticoid receptor-mediated mRNA decay, Sci. Adv. 7 (9) (2021), eabd9923.
[13] B. Yao, T. Hu, X. Cui, W. Song, X. Fu, S. Huang S, Enzymatically degradable alginate/gelatin bioink promotes cellular behavior and degradation in vitro and in vivo, Biofabrication 11 (4) (2019), 045020.
[14] A.C. Daly, M.E. Prendergast, A.J. Hughes, J.A. Burdick, Bioprinting for the biologist, Cell 184 (1) (2021) 18.
[15] A.C. Daly, M.D. Davidson, J.A. Burdick, 3D bioprinting of high cell-density heterogeneous tissue models through spheroid fusion within self-healing hydrogels, Nat. Commun. 12 (1) (2021) 753.
[16] J.A. Brassard, M. Nikolaev, T. Hübscher, M. Hofer, M.P. Lutolf, Recapitulating macro-scale tissue self-organization through organoid bioprinting, Nat. Mater. 20 (1) (2021) 22.
[17] B.R. Seo, X. Chen, L. Ling, Y.H. Song, A.A. Shimpi, S. Choi, J. Gonzalez, J. Sapudom, K. Wang, R.C. Andresen Eguiluz, D. Gourdon, V.B. Shenoy, C. Fischbach, Collagen microarchitecture mechanically controls myofibroblast differentiation, Proc. Natl. Acad. Sci. U. S. A. 117 (21) (2020) 11387.
[18] R. Wang, Y. Wang, B. Yao, T. Hu, Z. Li, Y. Liu, X. Cui, L. Cheng, W. Song, S. Huang, X. Fu, Redirecting differentiation of mammary progenitor cells by 3D bioprinted sweat gland microenvironment, Burns Trauma 7 (2019) 29.
[19] N. Ali, M. Hosseini, S. Vainio, A. Taïeb, M. Cario-André, H.R. Rezvani, Skin equivalents: skin from reconstructions as models to study skin development and diseases, Br. J. Dermatol. 173 (2) (2015) 391.
[20] Y. Zhang, Enhejirigala, B. Yao, Z. Li, W. Song, J. Li, D. Zhu, Y. Wang, X. Duan, X. Yuan, S. Huang, X. Fu, Using bioprinting and spheroid culture to create a skin model with sweat glands and hair follicles, Burns Trauma 9 (2021) tkab013.